Cavitation in flow through a micro-orifice inside a silicon microchannel

Cite as: Phys. Fluids **17**, 013601 (2005); https://doi.org/10.1063/1.1827602
Submitted: 21 June 2004 . Accepted: 05 October 2004 . Published Online: 14 December 2004

Chandan Mishra, and Yoav Peles

Cavitation in flow through a micro-orifice inside a silicon microchannel

Chandan Mishra and Yoav Peles[a)]
Department of Mechanical, Aerospace and Nuclear Engineering, Rensselaer Polytechnic Institute, Troy, New York 12180

(Received 21 June 2004; accepted 5 October 2004; published online 14 December 2004)

Hydrodynamic cavitation in flows through a micro-orifice entrenched in a microchannel has been detected and experimentally investigated. Microfabrication techniques have been employed to design and develop a microfluidic device containing an 11.5 μm wide micro-orifice inside a 100.2 μm wide and 101.3 μm deep microchannel. The flow of de-ionized water through the micro-orifice reveals the presence of multifarious cavitating flow regimes. This investigation divulges both similarities and differences between cavitation in micro-orifices and cavitation in their macroscale counterparts. The low incipient cavitation number obtained from the current experiments suggests a dominant size scale effect. Choking cavitation is observed to be independent of any pressure or velocity scale effects. However, choking is significantly influenced by the small stream nuclei residence time at such scales. Flow rate choking leads to the establishment of a stationary cavity. Large flow and cavitation hysteresis have been detected at the microscale leading to very high desinent cavitation numbers. The rapid transition from incipient bubbles to choking cavitation and subsequent supercavitation suggests the presence of radically different flow patterns at the microscale. Supercavitation results in a thick cavity, which extends throughout the microchannel, and is encompassed by the liquid. Cavitation at the microscale is expected to considerably influence the design of innovative high-speed microfluidic systems. © *2005 American Institute of Physics*. [DOI: 10.1063/1.1827602]

I. INTRODUCTION

The pernicious effect of hydrodynamic cavitation on conventional fluid machinery has been recognized and actively researched in the last century.[1–9] Cavitation in hydraulic machinery can limit performance, lower efficiency, introduce severe structural vibration, generate acoustic noise, choke flow, and cause catastrophic damage.[10–14] The present cavitation knowledge (experimental and analytical) has contributed immensely towards improving the design of conventional scale fluid machinery. The last decade has witnessed a surge in the development of MEMS (micro-electro-mechanical systems) and microfluidic systems[15–18] primarily due to the recent advancements made in microfabrication techniques.[19] The drive towards miniaturization of existing systems coupled with the vast potential of microfluidic systems for use in novel applications spread across diverse technological disciplines has resulted in the development of microrockets,[20–24] microengines,[25–27] microcoolers,[28–30] microrefrigerators,[31] microsatellites and nanosatellites,[32–34] drug delivery systems,[35] micropower systems including launch vehicles, high density power sources, electronic chip cooling systems, chemical microreactors,[36–38] DNA synthesis and bio-MEMS systems.[39–41] Any fluid handling device is vulnerable to cavitation once apposite hydrodynamic conditions are encountered.[3,4,42] Therefore, microfluidic systems are susceptible to the deleterious effects of cavitation if appropriate hydrodynamic conditions develop. Evidence of cavitation has been reported in MEMS turbopumps developed specifically for microrocket engines by Pennathur[43] and Pennathur *et al.*[44] Clearly, cavitation effects cannot be ignored in the design of microfluidic devices and a design framework needs to be established to facilitate the pragmatic realization of these novel microdevices. Literature review suggests that exceedingly limited cavitation research has been conducted for microscale devices. Pennathur *et al.*[44] conducted cavitation studies for a specific hydrofoil cascade but the devices used in their work were in the millimeter scale.

Although concomitant scaling effects of cavitation have been investigated,[45–52] they are mostly applicable in scaling between prototypes and real-world models at the conventional scale. Holl and Wislicenus[46] report that different sizes of hydrofoils produce different cavitation inception numbers thereby making cavitation scaling at the macroscale a very arduous affair. Moreover, the nuclei distribution and the diminished residence time (Brennen[2]) for growth of the nuclei at the microscale can significantly influence cavitation. It is to be noted that almost all microfluidic devices are fabricated using silicon, which is different from the material used in conventional scale hydraulic machinery. Holl[42] suggested that the source of cavitation is influenced by the surface energy characteristic (hydrophobic and hydrophilic) of the paragon. Since microfluidic devices are fabricated using silicon, which possesses vastly different properties than the materials used in large scale hydraulic devices, it is not appropriate to extend the present knowledge on cavitation at the large scale to design microdevices. Besides, research in microfluid flows has yielded unexpected results and deviations from conventional scale flow behavior.[15–18,53,54] Conse-

[a)]Author to whom correspondence should be addressed. Telephone: 518-276-2886. Fax: 518-276-2623. Electronic mail: pelesy@rpi.edu

quently, there is a strong need for an investigation of cavitation in microfluidic devices.

Micro-orifices are often encountered in microfluidic systems such as micropumps,[55–59] microvalves,[60–63] microcoolers, microreactors, microrefrigerators, etc. Recent publications have also reported the development of novel applications using micro-orifices such as the formation of dispersions and emulsions[64] and microdiesel injectors.[65] Lee *et al.*[66] studied gas flows through micro-orifices with a diameter of 10 μm and observed flow separation due to the constriction element. Hasegawa *et al.*,[53] in recent experiments on liquid flows through micro-orifices less than 35 μm wide, have detected pressure drops four times higher than those predicted by numerical analysis. However, only single-phase flows have been considered in their work.

Cavitation in conventional orifices has been investigated by many researchers.[67–80] The presence of a strong scale effect has been observed in the experiments of Yan and Thorpe,[67] Ramamurthi and Nandakumar,[73] Tullis and Govindarajan,[70] and Tullis[80] but no physical explanation has been offered for the same. Furthermore, the orifices used in previous studies[67–80] are in the millimeter scale and are not applicable to any MEMS devices. Also, microfluidic devices often have orifices with a rectangular cross section and almost all the research work done at conventional scales are for circular orifices. Billet and Holl[51] have hypothesized significant cavitation hysteresis effects at small scales but no experimental or analytical work has been conducted at the microscale and no data is available to make any conclusion.

The present investigation seeks to study hydrodynamic cavitation in an 11.5 μm wide micro-orifice entrenched in a 100.2 μm wide and 101.3 μm deep microchannel. The ulterior motive of this work is to identify and establish differences between cavitation in microscale and conventional scale orifices, assess the impact of cavitation on flows through a micro-orifice, detect differences in cavitating flow regimes, and enhance the understanding of cavitating flows through microchannels. It also aims to serve as a launching pad for future research on cavitation inside microfluidic systems. A brief review on cavitating flow through orifices is provided in Sec. II. The design and fabrication of the micro-orifice is presented in Sec. III, while the experimental setup description and the experimental procedure are provided in Sec. IV. Sections V and VI are devoted to the discussion of the experimental results and Sec. VII presents the conclusions of this investigation.

II. BACKGROUND

A. Flow through orifices

Fluid flow through orifices is characterized by a significant drop in the static pressure right after the orifice. The hydraulic grade lines (HGL) for flow through an orifice are shown in Fig. 1. A sharp pressure drop is observed downstream of the micro-orifice because of the sudden reduction in the flow area. The large pressure drop is primarily due to the generation and dissipation of eddies in the high shear layer around the submerged jet emerging from the orifice into the microchannel. The reduction in static pressure is

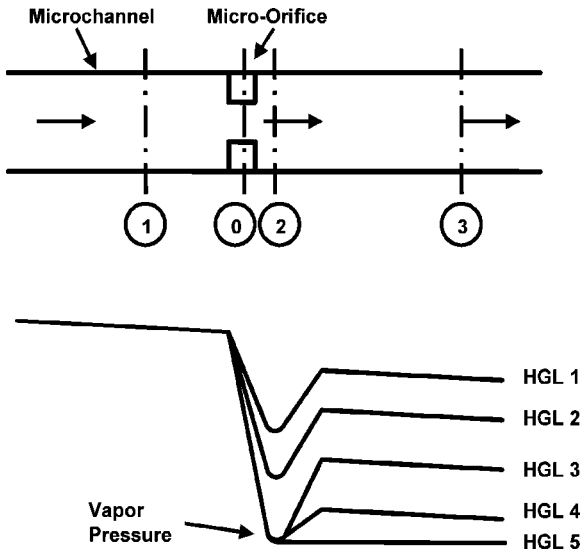

FIG. 1. Flow through an orifice and the hydraulic grade line (HGL) at various exit pressures.

accompanied by an acceleration of the fluid and a subsequent increase in the fluid velocity between points 1 and 2. The location (point 2) where the static pressure drops to its minimum and the velocity rises to its maximum, is termed the Vena Contracta. Therefore, large dynamic heads are present at the orifice throat (Vena Contracta) and can cause the static pressure to fall to a very low value. The pressure at the Vena Contracta can be estimated using Bernoulli's equation if the contraction coefficient is known and no losses are assumed. The static pressure recovers downstream of the orifice as the submerged jet is dissipated by viscous shear and the pressure at point 3 can be calculated using the conservation of momentum principle. Any further static pressure losses are primarily due to friction since the channel area remains constant.

B. Cavitation in flow through orifices

The rudimentary requirement for hydrodynamic cavitation to appear is the reduction of static pressure to a critical value. This can be achieved by dramatically changing the area of a microchannel by introducing a micro-orifice in the flow field. A variety of cavitating and noncavitating flow regimes are encountered as the exit pressure is brought down. A reduction in the exit pressure is accompanied by a reduction in the static pressure at the Vena Contracta (HGL 1). The discharge is directly proportional to the square root of the pressure difference between points 1 and 2. Proceeding on similar lines and reducing the exit pressure results in lowering the static pressure at the Vena Contracta, and produces a concomitant increase in the discharge (HGL 2). When the Vena Contracta pressure reaches a critical value, it promotes the growth of nuclei (submicron bubbles) by diffusion of dissolved gas into the available nuclei. The static pressure is still above the vapor pressure of the liquid therefore the mechanism of bubble growth is dominated by gaseous cavitation. Further reduction of the exit pressure succeeds in lowering the static pressure at the Vena Contracta to

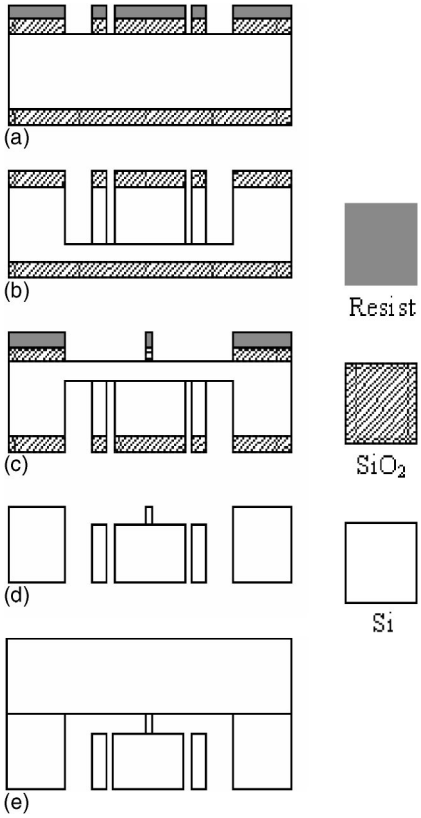

FIG. 2. Microfluidic device fabrication process flow. (a) Backside photolithography and RIE etching. (b) Backside DRIE to form pressure ports, fluid inlet, and exit ports. (c) Flip wafer, perform topside photolithography and RIE. (d) Topside DRIE to form the microchannel and the micro-orifice. (e) Silicon wafer packaged by anodic bonding with Pyrex wafer.

the vapor pressure of the liquid (HGL 3) and forms a vapor cavity. After this physical limit has been reached, any further attempt to increase the flow rate by reducing the exit pressure is ineffective. This is defined as choked flow or choked cavitation and the exit pressure loses its control over the discharge. The micro-orifice produces its maximum discharge under these conditions. Continuing to reduce the exit pressure only results in the elongation of the vapor cavity (HGL 4, HGL 5) and the orifice is said to be supercavitating.

III. MICRO-ORIFICE DESIGN, FABRICATION, AND PACKAGING

A. Microfluidic device fabrication

The first task in this investigation is to design and fabricate a microfluidic device capable of being used in cavitation experiments. The microfluidic device used in the present investigation consists of a micro-orifice entrenched inside a 2500 μm long microchannel. The device is microfabricated with techniques adapted from semiconductor manufacturing and the important steps in the process flow are presented in Fig. 2. A double side polished, *n*-type $\langle 100 \rangle$ single crystal silicon wafer is processed on both sides to create the microfluidic device. A 1 μm thick high quality thermal oxide is deposited on both sides of the silicon wafer to protect the bare wafer surface during processing. The backside of the silicon wafer is then taken through a photolithography step and an oxide removal process (reactive ion etching[19]) to mask and protect certain areas on the wafer that are not to be etched [Fig. 2(a)]. The wafer is then etched in a DRIE (deep reactive ion etching[19]) process and silicon is removed from places not protected by the photoresist/oxide mask. The DRIE process forms deep vertical trenches on the silicon wafer with a characteristic scalloped sidewall possessing a peak-to-peak roughness of ~ 0.3 μm. These trenches are deliberately created to serve as the device fluid inlet, fluid outlet, and the pressure port taps for the transducers [Fig. 2(b)]. Once the backside processing is completed, the photoresist is stripped and the wafer is flipped for topside processing. Photolithography and RIE (reactive ion etching) steps, similar to the steps used in the backside processing, are employed to create a mask on the topside of the silicon wafer. As before, a Bosch process (DRIE) is employed to remove silicon from the unprotected regions resulting in the creation of a microchannel containing a micro-orifice [Fig. 2(c)]. The DRIE process is continued until the wafer is etched through [Fig. 2(d)]. A mechanical stylus profilometer is used to determine the depth of the microchannel. Finally the processed wafer is Radio Corporation of America (RCA) cleaned and anodically bonded to a 1 mm thick polished Pyrex (glass) wafer to create a sealed device with an inlet, an outlet, and a few pressure ports [Fig. 2(e)]. After the successful completion of the bonding step, the processed wafer is die-sawed to produce individual test devices, which are subsequently packaged and interfaced with the experimental setup. The actual device is shown in Fig. 3(a) and an exploded two-layer computer-aided design (CAD) model is presented in Fig. 3(b) for completeness. Pyrex has been chosen as the top layer because it is transparent and will allow flow visualization. Since our experiments on cavitation involve visual inspection of the microchannel, it is mandatory to choose a material which is transparent and can provide a lucid view of the phenomenon.

B. Device packaging and instrumentation interface design

The fabricated microdevice needs to be packaged appropriately to facilitate the transit of fluids from the outside world and allow in-line pressure measurements. Therefore, a mechanical packaging module is designed to create an interface for the microfluidic device with the experimental setup and the associated instrumentation. The packaging module consists of three components: (a) a top transparent plate, (b) a bottom plate with alignment pins, and (c) an adapter plate. An exploded CAD model of the packaging module is shown in Fig. 4(a).

The bottom plate houses a few elastomeric gaskets (O-ring's) and the alignment pins facilitate the positioning of the MEMS device. The adapter plate compensates for any die-saw errors and allows flexibility in accommodating micro devices of different sizes. The transparent polycarbonate top plate allows flow visualization, which is a required criterion in the experiments. The silicon device is compressed against the elastomeric gaskets by the top and the bottom plate to forge the fluidic seals. This setup ensures hermetic sealing

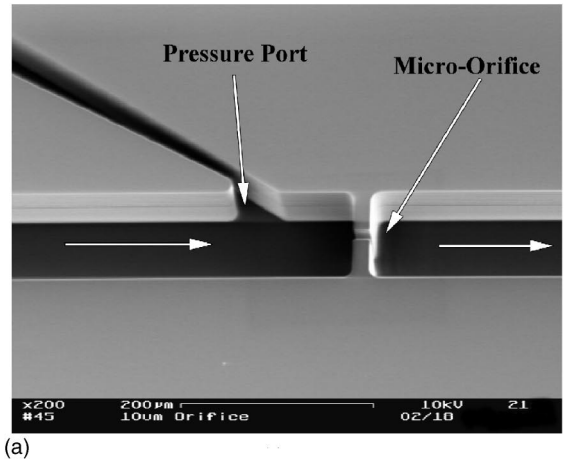

FIG. 3. (a) Scanning electron microscope image of micro-orifice. (b) CAD model of the microfluidic device. D_h is the hydraulic diameter of the microchannel.

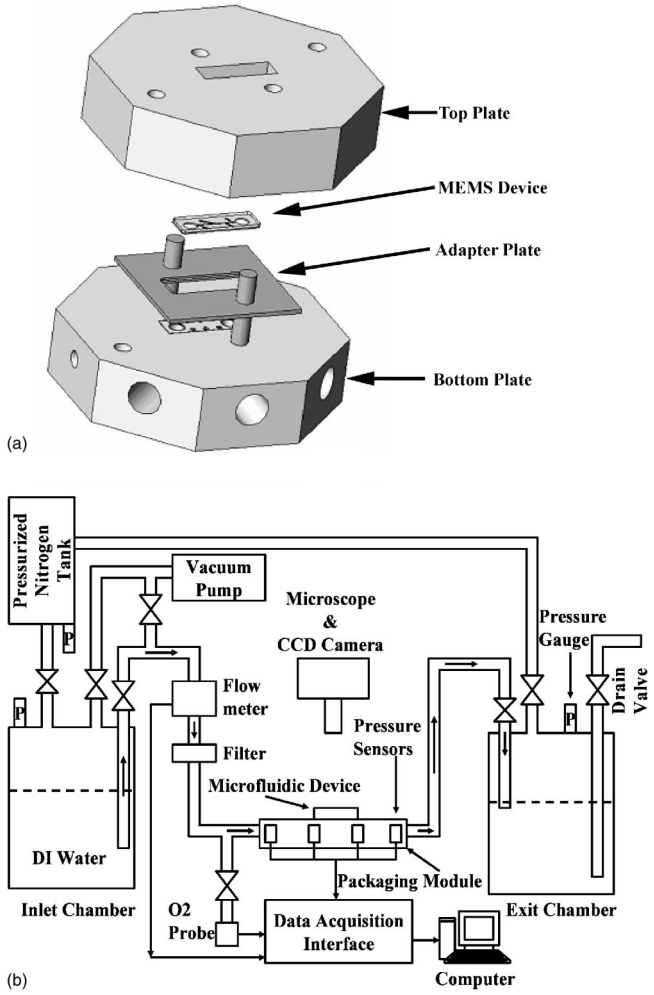

FIG. 4. (a) Exploded view of the packaging module assembly. (b) Experimental setup.

and offers access to the fluidic connections (inlet, outlet, and pressure ports) of the microdevice through the bottom block.

IV. EXPERIMENTAL SETUP DESIGN AND PROCEDURE OUTLINE

A. Experimental setup

Once the microfluidic device is packaged, the entire assembly is placed on an experimental rig shown in Fig. 4(b). The experimental setup is classified into three primary subsystems: (a) the flow subsystem, (b) the instrumentation and data acquisition subsystem, (c) the visualization and microscope subsystem.

The flow subsystem includes an inlet and an exit pressure chamber capable of withstanding pressures up to 190 psi. The fluidic connections to the packaging module from the pressurized tanks are established through vacuum fittings. The chambers are pressurized with filtered dry nitrogen. Filtered de-ionized water (DI water) has been used as the working fluid in all the experiments. The DI water is delivered through a 0.2 μm filter to remove any particles that might clog the micro-orifice, while the flow rate measurements are acquired from a calibrated flow meter. Air is removed from the flow circuit by a Welch vacuum pump before any DI water is introduced into the microchannel. Precision pressure transducers, mounted on the bottom plate of the packaging, are used to obtain and deliver pressure data at various locations in the microchannel to a personal computer (PC) based LabView® data acquisition subsystem for further analysis. Information from the pressure transducer located $30D_h$ downstream [Fig. 3(b)] of the micro-orifice is used for calculating the cavitation number. Visual data and images of cavitation and various cavitation flow regimes are captured by the charged-coupled device (CCD) camera mounted over a MEIJI EMZ-TR microscope. Finally, a calibrated commercial dissolved oxygen sensor (Omega DOB-215) is used to measure the concentration of dissolved oxygen in the working fluid. The dissolved oxygen concentration (DOC), an important parameter in cavitation experiments, is continuously monitored and measured during the experiments. The working liquid is not recirculated in any of the experiments to prevent the cavitation bubbles formed during a test run from reentering the test section.

B. Experimental procedure

The flow rate is controlled by the pressure difference between the inlet and exit chambers. Experiments are conducted over a wide range of inlet and exit pressures. In Phase-I of the experiments, the inlet chamber is kept at a fixed pressure and filtered DI water with a DOC of 8.7 ppm

TABLE I. Experimental uncertainties.

Physical parameter	Average uncertainty (%)
P_1	0.25
P_3	0.25
ΔP	0.67
Q	1
A_0	3.4
Re_h	1.11
C_O	1.2
σ	7.18

is allowed to flow through the micro-orifice. The exit chamber pressure is brought down in a controlled manner by employing a pump. Pressure and flow rate data are collected from various sensors at different exit pressure conditions. The microchannel is continuously scrutinized using a CCD camera mounted on a microscope and images of various cavitating flow regimes are procured. This information is simultaneously entered into the LabView® interface, while collecting the pressure and flow data. Under favorable hydrodynamic conditions, cavitation events commence and the corresponding images are recorded. In Phase-II, the pressure in the exit chamber is gradually increased by introducing nitrogen gas. As before, pressure, flow, and visual data is collected for a variety of exit pressures. All the above steps are repeated for different inlet chamber pressures to generate data for evaluating pressure scale effects. All the experiments are conducted at room temperature and the DI water temperature is continuously monitored. Phase-I and Phase-II experiments are repeated using DI water with different oxygen levels to assess the influence of dissolved oxygen on cavitation. In order to achieve a lower DOC (2 ppm), the inlet chamber, which stores the working fluid, is continuously vacuumed for 5–6 days. At such low pressures, the dissolved oxygen diffuses out and is removed by the vacuum pump. Higher DOC (15.4 ppm) is obtained by bubbling high-pressure oxygen in the chamber for 5–7 days. An error analysis, based on the standard methodology proposed by Kline and McClintock,[81] is employed to calculate the uncertainties associated with our experiments and the results are summarized in Table I.

C. Definitions/preliminaries

1. Hydraulic diameter

The microchannel and the micro-orifice used in the present study possess a rectangular cross section. In order to make any meaningful comparison with circular orifices, frequently encountered in macroscale flows, a hydraulic diameter must be employed. The hydraulic diameter of the micro-orifice is defined as

$$d_h = 4A_0/p_0. \tag{1}$$

Here, A_0 is the cross-sectional area of the rectangular micro-orifice and p_0 is the perimeter of the rectangular cross section.

2. Orifice discharge equation

The discharge through an orifice subjected to a pressure differential is defined as

$$Q = C_O A_0 \sqrt{\frac{2\Delta P}{\rho\left[1-\left(\frac{A_0}{A_p}\right)^2\right]}}, \tag{2}$$

where Q is the volumetric flow rate, A_p is the cross-sectional area of the microchannel, ρ is the density of water at 22 °C, and $\Delta P = P_1 - P_3$ is the pressure difference between the inlet and exit pressures prevailing in the microchannel (Fig. 1). C_O is the orifice discharge coefficient based on the pressure difference observed between P_1 and P_3. Due to the inherent difficulties in locating and measuring pressures right at the Vena Contracta, the readily available exit pressure P_3 is used to calculate the pressure differential. For small values of A_0/A_p, which is the case for the present device, $1-(A_0/A_p)^2 \approx 1$. Hence, Eq. (2) reduces to

$$Q = C_O A_0 \sqrt{\frac{2\Delta P}{\rho}}. \tag{3}$$

3. Reynolds number

The Reynolds number for flow through a micro-orifice is defined as

$$\mathrm{Re}_h = \frac{\rho V_0 d_h}{\mu}, \tag{4}$$

where μ is the dynamic viscosity of DI water at room temperature. The velocity V_0 is the mean velocity at the micro-orifice throat and is given by Q/A_O. A mean velocity is chosen in the above definition since it is not currently possible to measure velocities at the Vena Contracta without modifying the flow properties. Micro-PIV (particle image velocimetry)[82,83] offers possibilities to undertake such measurements but current technology lacks a methodology needed to produce any meaningful results at the high velocities (18–27 m/s) encountered in the current research.

4. Cavitation number σ

In order to quantify dynamically similar cavitating conditions and to represent the intensity of cavitation, a dimensionless parameter called the cavitation number has been widely employed. The orifice cavitation number[67] is defined as

$$\sigma = \frac{P_3 - P_v}{\frac{1}{2}\rho V_0^2}, \tag{5}$$

where P_v is the liquid vapor pressure. This definition provides a dimensionless platform to quantify, compare, and identify various stages of cavitation.

V. RESULTS AND DISCUSSIONS

Multifarious experiments on the flow of DI water through micro-orifices are conducted under a variety of conditions stretching from single-phase to supercavitating flows.

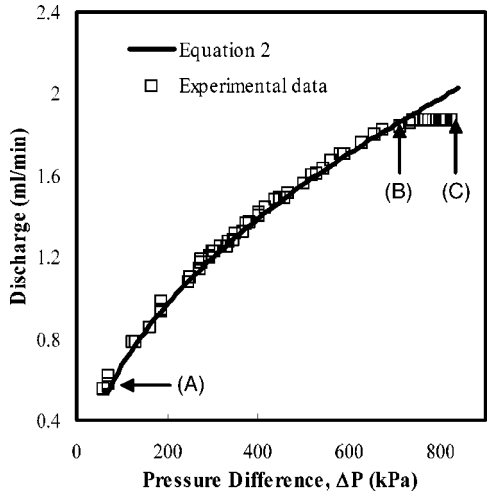

FIG. 5. Plot of discharge vs pressure drop.

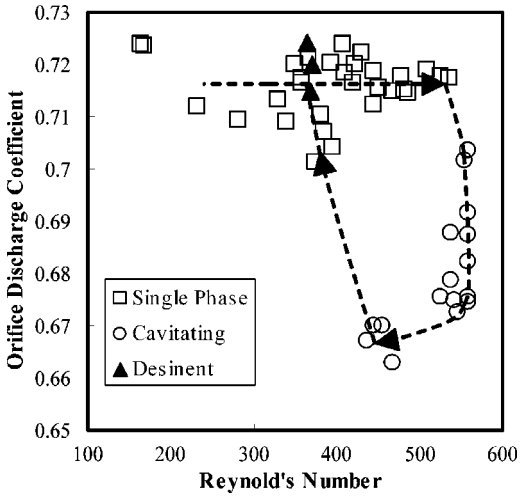

FIG. 6. Plot of discharge coefficient vs Reynolds number for single-phase and cavitating flows through a micro-orifice.

The reduction in the cavitation number causes an increase in the intensity and the extent of cavitation in the microchannel and unveils different cavitating flow regimes. An attempt has been made in subsequent sections to identify and characterize the different flow regimes encountered during this investigation.

A. Single-phase flow

A plot between volumetric flow rate Q and the pressure difference ΔP is presented in Fig. 5 using data obtained from Phase-I of the experiments. The region between A and B in Fig. 5 is single-phase and no cavitation bubbles are present at any time. The region contained between B and C corresponds to cavitating flows of various intensities. In the region between A and B, an increase in the pressure difference between the inlet and exit of the microchannel produces a corresponding increase in the flow rate. The trend from the experimental data shown in Fig. 5 suggests a quadratic relationship between the flow rate and ΔP. This is consistent for flows through an orifice inside a pipe and can be completely explained by Eq. (3). A large pressure drop is observed downstream of the micro-orifice, the reasons of which have been explained earlier. This suggests that single-phase flow through micro-orifices is similar to the flow observed through larger orifices inside pipes.

The discharge coefficient, calculated using Eq. (3), is plotted in Fig. 6. The discharge coefficient is found to be constant during single-phase flow for different pressure drops and Reynolds number. The analytical solution using a mean value of C_O, obtained from experiments, matches well with the data in the single-phase region (AB) as shown in Fig. 5. However, as expected it diverges from the experimental data in the cavitating region (BC). No anomalies have been detected in this investigation for the pressure drop in single-phase flows through micro-orifices contrary to the results presented by Hasegawa *et al.*[53]

B. Cavitation inception

After point B (Fig. 5) has been reached, any further reduction in the exit pressure (in an effort to increase ΔP) produces a marginal increase in the flow rate. Also, tiny, fast moving bubbles are detected downstream of the micro-orifice. If the static pressure at the Vena Contracta falls to a lower value, it promotes the growth of cavitation bubbles by the diffusion of dissolved gases into the submicron stream and surface nuclei. As is evident from Fig. 5, once cavitation has been initiated, the flow rate diverges from the calculated values using Eq. (3) with a constant C_O. In this investigation cavitation inception is defined as the initial appearance of bubbles accompanied by intermittent flashing due to appearance and disappearance of cavitation bubbles. Similar definitions of cavitation inception have been employed by various authors in the past.[2,3,84–86] The exit pressure is gradually reduced until initial bubbles appear 2–5 microchannel diameters downstream of the micro-orifice and the bubbles are detected with a microscope. This condition is termed as inception and a change in the flow regime from single-phase to bubbly cavitating flow is observed.

The cavitation inception number σ_i obtained from the present experiments (Table II) is considerably lower than any previous macroscale studies[67,70,73,75,80] suggesting a strong scale effect, which had earlier been hypothesized by Yan and Thorpe.[67] The small values of σ_i maybe attributed to the small residence time of the bubble due to the relatively high velocities of the fluid and the small size of the micro-orifice.

TABLE II. Various cavitation data for the micro-orifice.

Cavitation parameter description	Mean value of parameter
Incipient cavitation number	0.284
Choked cavitation number (experiments)	0.242
Choked cavitation number (analytical solution $Cc=0.62$)	0.34
Desinent cavitation number	3.644

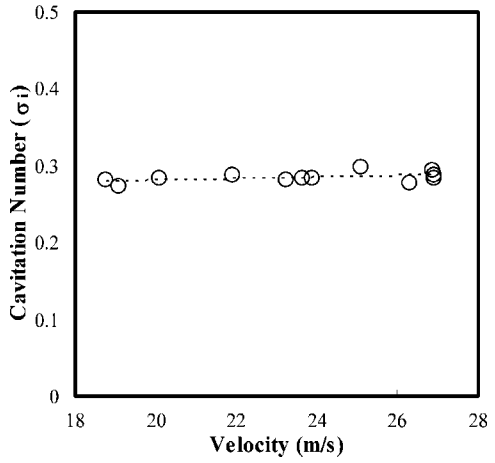

FIG. 7. Velocity scale effects on incipient cavitation number.

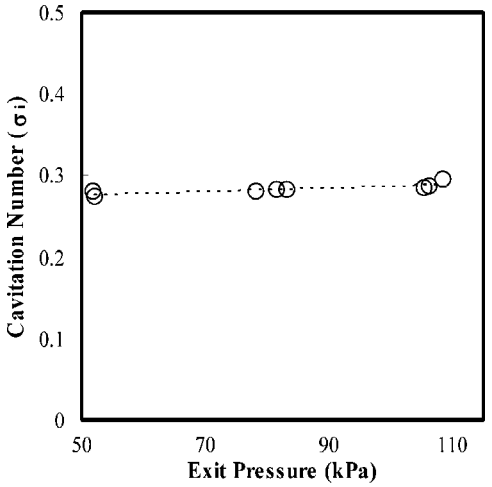

FIG. 8. Pressure scale effects on cavitation inception number.

Also at such small scales, surface tension forces are significant and can delay the rupture of the liquid. Therefore, the exit pressure has to be reduced to a relatively lower value before the first bubbles are detected in the microchannel. Cavitation inception is believed to occur primarily due to the diffusion of dissolved gases into the available nuclei.[3,4,67] The dynamic heads encountered during the appearance of the initial bubbles are not sufficient to lower the static pressure at the Vena Contracta to the vapor pressure. This leads us to believe that incipient cavitation or the first appearance of bubbles is dominated by gaseous cavitation. However, extremely low local pressures can exist due to the formation of eddies in the high shear layer just downstream of the orifice. These eddies can contribute to the growth and collapse of the bubbles. Therefore, in orifice flows, cavitation inception might be the result of both gaseous and vaporous cavitation. Once the static pressure at the Vena Contracta reaches vapor pressure, the mechanism of bubble growth is dominated by vaporous cavitation.

C. Velocity and pressure effects at inception

The cavitation inception number is determined at different velocities at the orifice throat V_0 and presented in Fig. 7. It is clear from Fig. 7 that the cavitation inception number is independent of any velocity scale effects. A similar phenomenon has been observed by Yan and Thorpe[67] in larger orifices.

Pressure effects on cavitation inception are studied by employing various inlet pressures and comparing the cavitation inception number with the prevalent exit pressures at inception. A plot (Fig. 8) for the exit pressure at inception reveals that the cavitation number σ_i remains unchanged for different inlet pressures. Therefore, it can be concluded that cavitation inception is independent of any pressure scale effects. A similar trend has been observed at conventional scales.[67,70,80] Figure 9 suggests that at inception the velocity and the exit pressure share a quadratic relationship. This is entirely expected since σ_i remains constant irrespective of the velocities or pressures. Since pressure scaling effects are absent at inception, the presented data is valid at any inlet pressure.

D. Choking cavitation

The flow rate continues to rise even after the initial bubbles are detected in the microchannel. However, the discharge deviates from the quadratic relationship established during single-phase flow (Fig. 5). Further reduction in the exit pressure lowers the cavitation number and increases the intensity and occurrence of cavitation events inside the microchannel. At a certain exit pressure, a single stationary cavity is observed $(2-4)D_h$ downstream of the micro-orifice. The exit pressure loses control over the flow rate once this condition has been realized. The flow rate saturates and remains constant completely ignoring the effects of the decreasing exit pressure. This predicament is defined as choked cavitating flow and flow rate saturation is descried irrespective of the inlet pressures (Fig. 10). The rise in intensity of cavitation events points to the establishment of a dominant vaporous cavitation mechanism.

Choking occurs even at conventional scales and has been reported by Yan and Thorpe,[67] Tullis,[69,80] and Bikai *et al.*[75] Nevertheless, at the microscale, the transition from incipient cavitation to the choking condition is rapid. A meager reduction in the cavitation number after inception results in

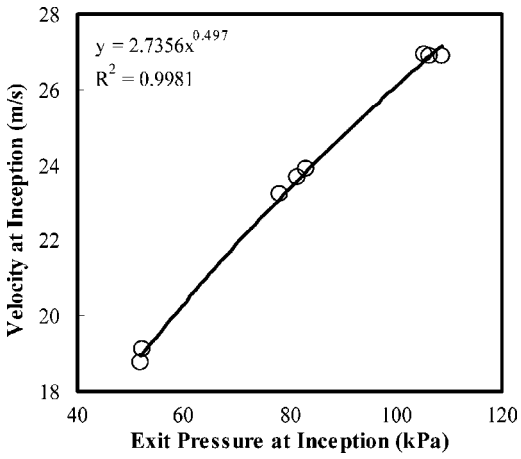

FIG. 9. Plot of velocity and pressure at cavitation inception.

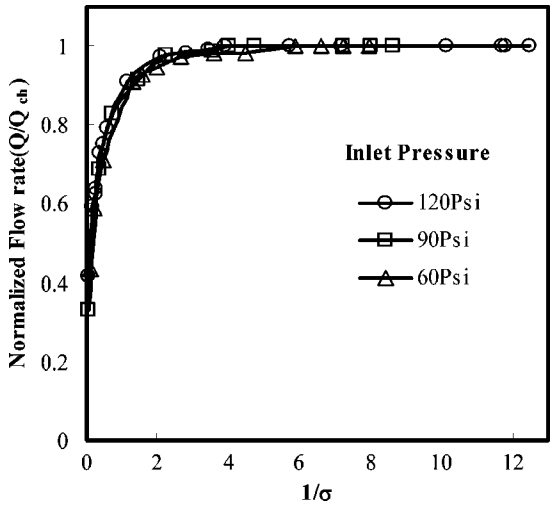

FIG. 10. Normalized discharge vs $1/\sigma$.

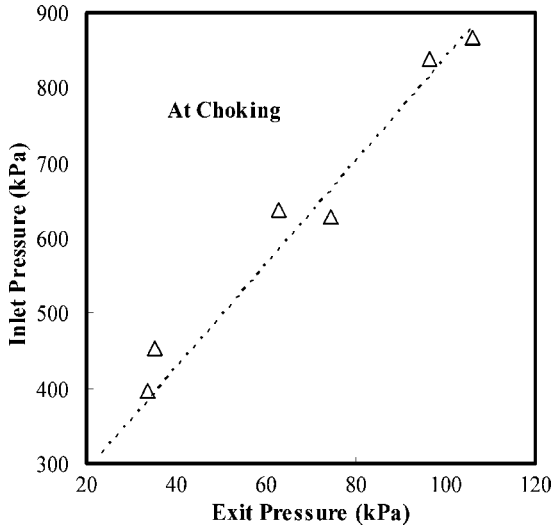

FIG. 11. Plot of inlet and exit pressures at flow rate choking.

choked cavitation at the microscale. In the experiments of Yan and Thorpe[67] and Tullis,[69,80] conducted on larger orifices inside larger pipes, the cavitation number had to be reduced significantly beyond inception before flow rate choking is detected. Table III summarizes the incipient and choking cavitation numbers for both micro and conventional scales and shows the rapid transition from incipient to choked cavitation in the case of a micro-orifice. Tullis[69] discloses a 59% increase in the flow rate beyond inception to cause choking, whereas in the present study only a 1–2% increase in the flow rate beyond inception is sufficient to cause choking. Therefore, at the microscale, once cavitation bubbles appear, there is a strong possibility of the flow rate being choked with the slightest reduction in the cavitation index. Also, in microflows, choking occurs with the formation of a single stationary vapor cavity downstream of the micro-orifice, which has not been reported in any previous studies.

1. Analytical expression for cavitation number at choking

Applying Bernoulli's equation between sections 1 and 2 (Fig. 1) and rearranging the terms gives

TABLE III. Comparison between choked cavitation numbers in microscale and large-scale.

	Macroscale[a] ($d_h=1.70\times10^{-2}$ m)	Macroscale[b] ($d_h=2.96\times10^{-2}$ m)	Microscale $d_h=(20.65\ \mu$m)
Incipient cavitation σ_i	1.95	1.10	0.284
Choking cavitation σ_{ch}	0.57	0.27	0.242

[a]Reference 67.
[b]Reference 68.

$$P_1 - P_2 = \frac{1}{2}\rho\left(\frac{V_1}{C_d}\right)^2\left[1-\left(\frac{A_2}{A_p}\right)^2\right], \tag{6}$$

where A_2 is the cross-sectional area at the Vena Contracta and C_d is the discharge coefficient based on the pressure difference $\Delta P = P_1 - P_2$. Employing the conservation of momentum principle between cross-section 2 and 3 the following is obtained:

$$P_2 - P_3 = \rho V_3^2\left(1-\frac{A_p}{A_2}\right). \tag{7}$$

Dividing Eq. (7) by Eq. (6) and observing that $P_2 = P_v$ at choking gives

$$\frac{P_3 - P_v}{P_v - P_1} = \frac{2C_d^2\left(\frac{A_0}{A_p}\right)^2\left(1-\frac{A_p}{A_2}\right)}{\left[1-\left(\frac{A_0}{A_p}\right)^2\right]}. \tag{8}$$

The dimensionless discharge plot (Fig. 10), for three different inlet pressures, shows that choking is independent of any pressure scale effects. This is consistent with conventional scale arguments that choking is a direct consequence of the development of vapor pressure at the orifice Vena Contracta.[67,80] Furthermore, a plot (Fig. 11) between the inlet and exit pressures at choking yields a linear relationship between P_1 and P_3, which is consistent with the experimental results of Yan and Thorpe.[67] Equation (8) also suggests that P_1/P_3 is constant at choking validating the experimental results.

An analytical expression for the cavitation number at choking is determined by substituting Eq. (8) in Eq. (5):

$$\sigma_{Ch} = 2\left(\frac{A_0}{A_p}\right)^2\left(\frac{A_p}{A_0}\frac{1}{C_C}-1\right), \tag{9}$$

where C_C is the contraction coefficient. A similar expression for choking cavitation has been derived in Yan and Thorpe[67] for circular orifices. An empirical ratio relating C_C to the area ratio (Daily and Harleman[72]) is given by

$$C_C = 0.62 + 0.38\left(\frac{A_0}{A_p}\right)^3. \tag{10}$$

Nurick[77] validated the above expression by conducting cavitation experiments on circular and rectangular orifices and observed that the contraction coefficient is independent of the orifice cross section. The analytical cavitation number at choking obtained from Eq. (9), and the experimental results are presented in Table II. The difference in the results are beyond the uncertainties associated with the experiments. The discrepancy can be attributed either to values of the contraction coefficient or the delay in the formation of the stationary cavity due to the small residence time for bubble growth or a combination of both. A literature survey reveals no information on the contraction coefficients at such small scales. One possible explanation to the above discrepancy is that the contraction coefficient in micro flows is slightly higher. Schmidt and Corradini[87] have employed $C_C=0.7$ in their one-dimensional (1D) cavitating orifice model and obtained reasonable results. Employing a higher contraction coefficient ($C_C=0.75$) in Eq. (9) yields choking cavitation numbers, which match the experimental results obtained in this investigation. This argument assumes that vapor pressure is present at the Vena Contracta during choking ($P_2=P_v$).

A second argument explaining the above discrepancy is based on the small residence time for bubble growth witnessed at such small scales. An expression for the inertially controlled bubble growth time based on the Rayleigh-Plesset equation has been developed in Brennen,[2] and is given by

$$t = R_0 \int_1^{R/R_0} \left[\frac{2(P_V - P_\infty)(1 - x^{-3})}{3\rho} + \frac{2P_{G0}(x^{-3k} - x^{-3})}{3(1-k)\rho} - \frac{2S(1 - x^{-2})}{\rho R_0 x} \right]^{-0.5} dx, \tag{11}$$

where $x=R/R_0$ and R_0, R, P_{G0}, P_∞, S, and k are the initial bubble size, final bubble size, partial pressure of noncondensable gas, driving pressure, surface tension, and the polytropic index, respectively. Bubble growth time is obtained by numerically solving Eq. (11) for an initial bubble radius of 1 μm to a final size of 10 μm for different values of the driving pressure, while ignoring the effects of the noncondensable gases. The calculated stream nuclei residence time in the micro-orifice is between 0.3–0.55 μs based on the velocities observed in our experiments. A driving static pressure of zero yields a growth time of 5.17 μs, which is an order of magnitude higher than the time spent by the stream nuclei in the micro-orifice. Only if the liquid is subjected to a tension[2] of 23.7 kPa (which corresponds to a negative absolute pressure of 21 kPa), the growth time reduces to the time scales (0.3–0.55 μs) observed in the present experiments. Therefore, it is apparent that the small residence time of the stream nuclei will almost definitely influence cavitation in microscale devices. Nevertheless, cavitation can be instigated due to other sources such as the surface nuclei. The surface nuclei might have the opportunity to reside for a longer time inside the micro-orifice and promote cavitation events. At the macroscale, numerous studies have revealed that the excitation of stream nuclei rather than surface nuclei dominates the onset of cavitation (Brennen[2]). This may no longer be true at the microscale, wherein the surface nuclei might dictate cavitation events. In any case, when the static pressure at the Vena Contracta drops to the vapor pressure, it forms a local low pressure region, which is limited in terms of size. The nuclei traveling through this low pressure region do not possess sufficient time to dwell and grow. Therefore, no cavity is formed and the liquid does not rupture. It has also been reported that surface tension at the microscale can assist the liquid to withstand high tensile stresses and resist rupture. A further reduction in the exit pressure extends the low pressure area beyond the Vena Contracta. When sufficient dwelling time (because of the increase in the low pressure region) is available for the nuclei to grow, a stationary cavity is established $(2-4)D_h$ downstream of the microchannel. Therefore, the choking cavitation numbers obtained from the present experiments are lower then the predicted values. Clearly, the nuclei residence time influences cavitation and its effects are pronounced at the microscale.

E. Supercavitation

Once choking develops, a thick vaporous cavity is detected throughout the microchannel [Fig. 12(a)]. The cavity is encompassed by the liquid and extends until the end of the microchannel (around $1400d_h$ downstream of the micro-orifice).This condition is termed supercavitation and a flow regime transformation is detected. Previous experiments by Yan and Thorpe[67] detected a supercavity encompassing a thick liquid jet. Therefore, the flow pattern observed during supercavitation at the microscale is different from those observed in larger orifices. Further, in microscale fluid flows the onset of choking proclaims the arrival of supercavitation. The appearance of the thick vapor cavity is transpicuous from Fig. 12(a). Upon reducing the cavitation number, the supercavity gets thicker as shown in Fig. 12(b). The supercavity tail is vivid even at the microchannel exit [Fig. 12(c)]. Once supercavitation is established, it can affect any component located at large distances downstream of the micro-orifice. Supercavitation is a potentially dangerous condition and can cause severe damage downstream of the supercavity (Tullis[69,80]). The MEMS test device used in this experiment suffered severe damage after being used for 120–150 h in cavitating conditions and the upper level Pyrex cover and the lower level silicon cracked downstream of the micro-orifice in the midst of a test run. Therefore, it is very clear that attention has to be paid to avoid supercavitating conditions in microfluidic devices. Additionally, a meticulous study on supercavitating conditions is required to understand its implications on device performance and assess any concomitant damage.

F. Flow hysteresis

After supercavitation has been reached, the exit pressure is raised (Phase-II) until the cavitation bubbles are no longer visible in the microchannel. A change in flow regime is observed from cavitating to single-phase flow. A plot between the flow rate and the pressure difference is presented in Fig. 13. Surprisingly, the flow rates observed in Phase-II of the

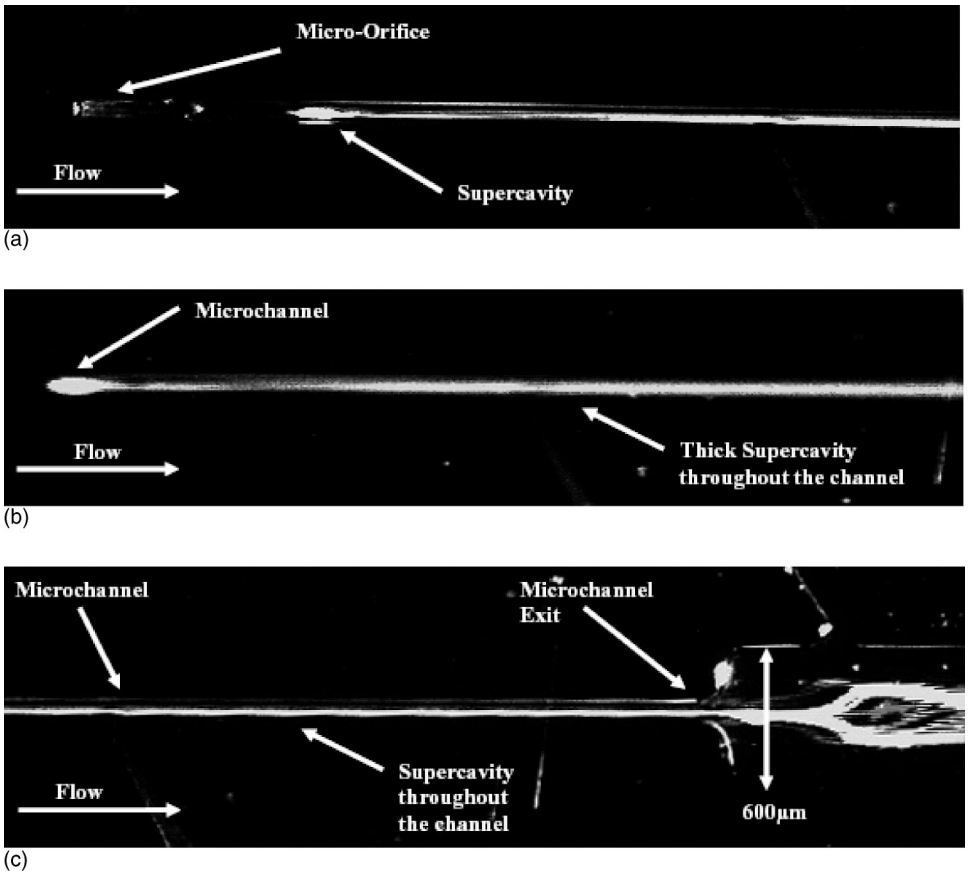

FIG. 12. (a) Supercavitation observed throughout the microchannel at $\sigma = 0.17$ (b) Supercavitation observed throughout the microchannel at $\sigma = 0.09$. (c) Supercavitating flow at the exit of the microchannel for $\sigma = 0.17$.

experiments are lower than the observed values in Phase-I for the same ΔP. Consequently, a significant flow hysteresis effect is detected at the microscale. The large cavitation hysteresis effect is due to the reluctance of cavitation bubbles to disappear even at higher cavitation numbers. The presence of a large vapor cavity during supercavitation prevents the increase in discharge by effectively reducing the area available for the liquid to flow. The high local velocity heads developed because of the reduction in flow area creates local low pressure conditions capable of sustaining the cavity. Any attempt to collapse the large stationary cavity by raising the exit pressure is overshadowed by these large local dynamic heads. The exit pressure has to be sufficiently increased before the cavity collapses and the flow returns to the single-phase regime. Therefore, it is extremely difficult to return to noncavitating conditions once the stationary cavity develops. At the microscale, cavitation hysteresis significantly influences the flow rate when a transition is made from cavitating to noncavitating flow regimes. Moreover, the exit pressure loses its control over the discharge during this transition. Designers of microfluidic systems need to be aware of this phenomenon as it can adversely affect device performance.

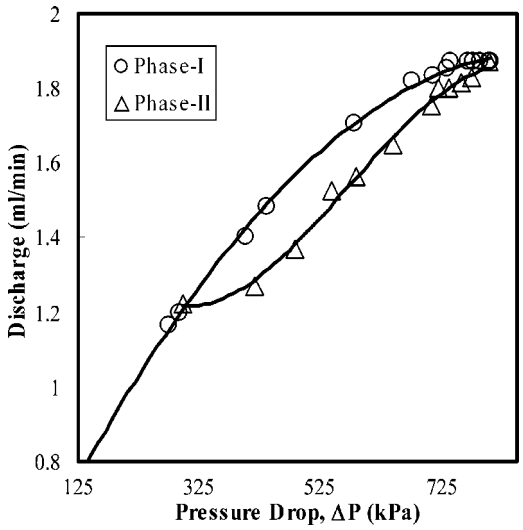

FIG. 13. Discharge vs pressure difference for Phase-I and Phase-II experiments.

G. Desinent cavitation

The desinent cavitation number is defined as the cavitation number at which the cavitation bubbles completely disappear as a result of raising the exit pressure.[3,88,89] This is often used as a threshold between cavitating and noncavitating flows. The value of desinent cavitation has been reported to be slightly higher than the incipient cavitation by various authors in previous cavitation studies at the macroscale. The current experiments reveal a much larger difference between the incipient and desinent cavitation numbers (Table II) suggesting a very strong scale effect. Such pronounced differences between incipient and desinent cavitation numbers have never been reported in conventional scale studies, although Hall and Treaster[88] had suspected that cavitation hysteresis effects would increase with a decrease in size of the

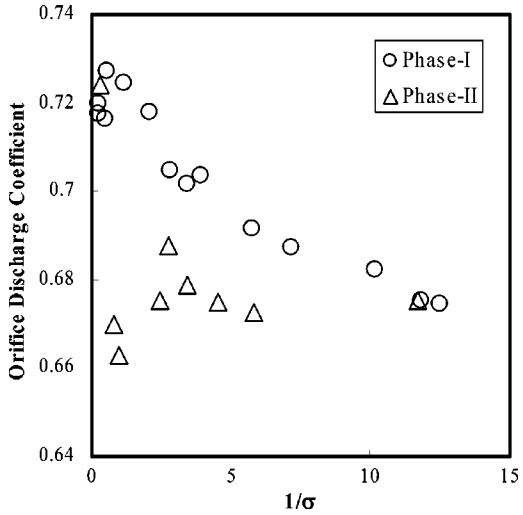

FIG. 14. Effect of cavitation number on the discharge coefficient.

archetype. The large difference in the cavitation number between incipient and desinent cavitation at the microscale leads us to believe that the flow patterns encountered in microscale cavitation are radically different from those observed at the macroscale. A high-speed camera study will certainly reveal interesting information about the prevalent flow patterns and ameliorate the understanding of microscale cavitating flows. Nevertheless, an important observation from the experimental data (Fig. 13) is that the relatively large cavitation hysteresis makes it extremely difficult to extirpate cavitation once it is instigated. Therefore, cavitation is still a concern in the design of microfluidic devices, and deserves serious consideration.

H. Effect of flow hysteresis on discharge coefficient

The discharge coefficient falls as the cavitation number is reduced. After reaching supercavitation, increasing the exit pressure does not have any effect on the discharge coefficient. The discharge coefficient continues to remain at the low levels observed during supercavitating flows even at higher exit pressures as shown in Figs. 6 and 14. Once the single-phase flow is achieved, the discharge rate returns to levels observed during single-phase flows.

I. Effects of dissolved oxygen concentration

The amount of oxygen present in the working fluid has been known to alter the cavitation inception number.[67,90,91] Therefore, is necessary to investigate the effects of DOC on microscale cavitation. Figure 15(a) shows that the incipient cavitation number for a DOC of 15.4 ppm is notably higher than the value obtained for a DOC of 8.7 ppm. The increase in the gas content promotes the growth of submicron bubbles through diffusion. Inception is greatly influenced by the initial diffusion of dissolved gases into subcritical nuclei and depends heavily on the availability of nuclei. Therefore, an increase in the availability of dissolved gas nuclei due to the high oxygen concentration leads to a higher cavitation inception number. Over the last 50 years, numerous other authors have detected a similar trend in larger prototypes.[3,90,91] This

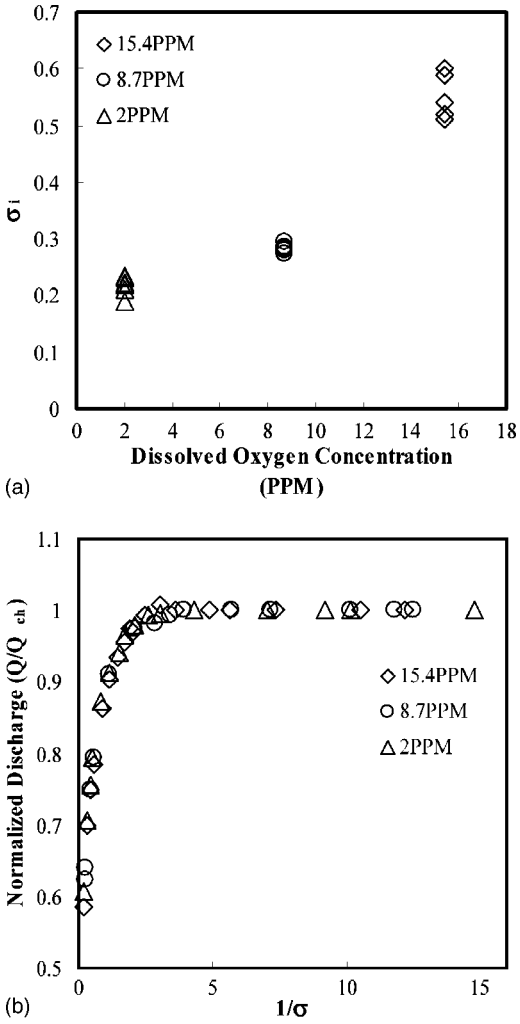

FIG. 15. (a) Effect of dissolved oxygen concentration on incipient cavitation number. (b) Effect of dissolved oxygen concentration on normalized discharge.

effect of the DOC on cavitation inception is supported by Yan and Thorpe[67] in their cavitation experiments conducted on larger orifices. The opposite happens when the DOC is reduced in the working fluid. Cavitation inception is delayed and the cavitation inception number is lower than the values obtained in phase I using DI water with a DOC of 8.7 ppm [Fig. 15(a)]. This lucidly shows that by reducing the dissolved gas nuclei in the working fluid the rupture of the liquid can be delayed thereby allowing the liquid to withstand higher tensile stresses prior to rupture. In addition, cavitation inception at a low DOC (2 ppm) displays a time delay, which has also been mentioned in the work by Holl and Treaster.[88] The initial bubbles showed up after 30–60 min of lowering the exit pressure and made the experiments painstakingly slow. The hypothesis by Holl and Treaster[88] that the time delay increases on the reduction of size and the DOC seems to match the observed trends in the present experiments. Also, when the DOC is very low (2 ppm), the flow chokes once cavitation is detected. Hence, at the microscale the appearance of cavitation will lead to choking of the flow rate provided the working liquid is pure

and degassed. Furthermore, the DOC seems to have no effect on choking, supercavitation, flow hysteresis, or the discharge rates [Fig. 15(b)].

VI. SIMILARITIES AND DEVIATIONS FROM MACROSCALE RESULTS

This investigation reveals differences and similarities between cavitation observed in fluid flow through micro-orifices and cavitation in their macroscale counterparts. Since fluid flows in MEMS devices have shown unexpected phenomena and deviations from established large scale results, the deviations shown in our experiments are not entirely unexpected. These experiments confirm the existence of certain scale effects and unveil effects which have not been suspected or reported in any previous studies. It is therefore appropriate to summarize both the similarities and dissimilarities observed between macroscale and microscale cavitation.

A. Similarities

The following are the similarities observed between macroscale and microscale cavitation.

(1) Single-phase flow though a micro-orifice is similar to those observed for large orifices. The discharge and the pressure drop observed in flows through a micro-orifice share a quadratic relationship, which has also been observed in larger orifices. The single-phase flow in both cases can be completely described by Eq. (2). The discharge coefficient remains constant during single-phase flow and is independent of any Reynolds number or size scale effects.

(2) A variety of flow regimes are encountered when the cavitation index is reduced. Incipient, choking, and supercavitating conditions have been detected in this study. Comparable flow regimes have been detected in experiments by Yan and Thorpe[67] on their macroscale counterparts, however, flow patterns are different.

(3) DOC in the working liquid has similar effects on cavitation at any scale. A larger σ_i is obtained when the DOC in the working fluid is higher, while a smaller σ_i is realized when the DOC is lower.

(4) The desinent cavitation number is always higher than the incipient cavitation at any scale although at the microscale, the difference between them is considerably large.

(5) No velocity or pressure scale effects have been detected at cavitation inception for either the micro-orifices or macro-orifices.

(6) The choking cavitation number is independent of any velocity or pressure scale effects and the DOC of the fluid does not affect choking at any scale. At choking, P_1/P_3 remains constant for a variety of inlet and outlet pressures and this trend is also observed in macroscale orifices.

(7) The orifice discharge coefficient falls when flow transitions from single-phase to two-phase cavitating flow.

(8) Cavitation is a destructive phenomenon and can cause damage and adversely affect the performance of both microhydraulic and macrohydraulic devices.

B. Deviations

The following are the dissimilarities observed between macroscale and microscale cavitation.

(1) The cavitation inception number obtained from our experiments on micro-orifices is much smaller than the values obtained from previous studies on larger orifices suggesting the presence of a strong size scale effect. This scale effect is possibly influenced by stream nuclei dwell time and surface tension forces, which are significant at such small scales. Therefore, a much larger effort is required to instigate cavitation at the microscale.

(2) At the microscale, cavitation is extremely difficult to eradicate once it develops. As a result, huge differences between the desinent and incipient cavitation numbers are observed. Cavitation hysteresis has also been reported in the macroscale flows but its effects are more pronounced at the microscale.

(3) The quick transition from incipient cavitation to choking cavitation in micro-orifices is in complete contrast to the trend observed in larger orifices.[67,69,70,80] The difference observed between σ_i and σ_{Ch} is much bigger at the macroscale. The incipient cavitation number is relatively small at the microscale and the transition to choking is accelerated. Moreover, the presence of a few vapor bubbles near the Vena Contracta is sufficient to choke the flow at such small scales.

(4) Choking of the flow rate is observed after the establishment of a stationary cavity $(2-4)D_h$ downstream of the micro-orifice. This has not been reported in any previous investigation on larger orifices. The choking cavitation number does not match the predicted results unlike the results obtained for larger scales. The small stream nuclei residence time coupled with the ability of the liquid to withstand low pressures without rupturing delays the formation of the stationary cavity and results in the above discrepancy.

(5) The onset of choking heralds the arrival of supercavitation at the microscale. In macroscale studies, the cavitation number has to be sufficiently lowered beyond choking conditions for supercavitation to develop. Also, supercavitation at the microscale results in a thick vaporous cavity engulfed by the liquid. The supercavity, which extends until the channel exit, is detected in the center of the microchannel. In larger orifices, a vapor cavity is observed encompassing a thick liquid jet, which breaks up after hitting the walls of the pipe downstream of the orifice. Hence, the supercavitating flow pattern observed for micro-orifices is radically different from those observed in studies on larger orifices.

(6) Large flow hysteresis is observed at the microscale. Once the cavitation bubbles are formed, they modify the flow rate since the bubble size is comparable with the micro-orifice or the microchannel dimension. Much lower flow rates are observed at the same pressure difference and a significant flow hysteresis is present. The large flow hysteresis causes the exit pressure to lose control over the discharge. This has never been a concern for designers of conventional scale hydraulic machinery.

(7) Surface nuclei, which are less dominant than the stream nuclei at the macroscale, are expected to have consid-

erable influence on cavitation at the microscale. Furthermore, the surface topography and chemistry are different in silicon MEMS devices.

(8) The materials used in MEMS/microfluidic devices are different from those used in fabricating hydraulic machinery in the macroworld. The damage characteristics in microfluidic devices will certainly be different and deserve a comprehensive investigation.

VII. CONCLUSION

Hydrodynamic cavitation has been revisited at the microscale. Cavitating flows through a micro-orifice have been experimentally investigated and results indicate the existence of strong scale effects. A comparison between microscale and macroscale results has been performed and both similarities and deviations have been observed. A variety of flow regimes, similar to those observed at larger scales, are encountered as the cavitation number is reduced. The incipient cavitation number obtained in the current experiments is very low suggesting a prevailing size scale effect. The flow rate chokes after the establishment of a single stationary cavity $(2-4)D_h$ downstream of the micro-orifice. The choked cavitation numbers in micro-orifice flows are lower than the predicted values. The ability of the liquid to withstand low pressures at such scales combined with an extremely small dwelling time for stream nuclei growth results in smaller choking cavitation numbers. Surface nuclei are believed to play a more active role in microscale cavitation. The choking cavitation number is independent of any velocity or pressure scale effects. Significant cavitation hysteresis[51] has been detected leading to large differences between σ_i and σ_d. Results also indicate a quick transition in the flow regimes from incipient to choking and subsequent supercavitation. Supercavitation produces a cavity, which is present through the entire length $(1400d_h)$ of the microchannel, and is surrounded by a liquid jet. It is extremely difficult to exterminate this supercavity once formed and this leads to high desinent cavitation numbers at the microscale. Surface tension forces, which are dominant at such scales, are suspected to be responsible for this phenomenon. The cavitating flow patterns present in microscale flows are radically different from those observed in their macroscale counterparts. Confirmation of their existence and a detailed understanding of the flow patterns can be achieved only by conducting investigations with a high-speed camera. The effect of dissolved oxygen concentration has also been investigated and the trends are very much in line with those observed at the macroscale. Cavitation is expected to significantly influence and limit the design of high-speed microfluidic machines and devices. The deleterious effects of cavitation damage, noise, and reduced efficiency are a matter of concern for designers of microscale devices. Design guidelines for MEMS fluid machinery need to be developed for the successful realization of these novel hydraulic micromachines.

ACKNOWLEDGMENTS

The microfabrication was performed in part at the Cornell NanoScale Facility (a member of the National Nanotechnology Infrastructure Network) which is supported by the National Science Foundation under Grant No. ECS-0335765, its users, Cornell University, and industrial affiliates.

[1] R. E. A. Arndt, "Cavitation in fluid machinery and hydraulic structures," Annu. Rev. Fluid Mech. **13**, 273 (1981).
[2] C. E. Brennen, *Cavitation and Bubble Dynamics* (Oxford University Press, Oxford, UK, 1995).
[3] R. T. Knapp, J. W. Daily, and F. G. Hammit, *Cavitation* (McGraw-Hill, New York, 1970).
[4] M. S. Plesset, "The dynamics of cavitation bubbles," J. Appl. Mech. **16**, 277 (1949).
[5] L. Rayleigh, "On the pressure developed in liquid during the collapse of spherical cavity," Philos. Mag. **34**, 94 (1917).
[6] F. R. Young, *Cavitation* (McGraw-Hill, New York, 1989).
[7] E. N. Harvey and W. D. McElory, "On the cavity formation in water," J. Appl. Phys. **18**, 162 (1947).
[8] D. D. Joseph and A. Prosperetti, "Cavitation and the state of stress in a flowing liquid," J. Fluid Mech. **366**, 367 (1998).
[9] B. Ran and J. Katz, "The response of microscopic bubbles to sudden changes in the ambient pressure," J. Fluid Mech. **224**, 91 (1991).
[10] Y. Tomita and A. Shima, "Mechanisms of impulsive pressure generation and damage pit formation by bubble collapse," J. Fluid Mech. **169**, 535 (1986).
[11] J. R. Blake and D. C. Gibson, "Cavitation bubbles near boundaries," Annu. Rev. Fluid Mech. **19**, 99 (1986).
[12] A. Karimi and F. Avellan, "Comparison of erosion mechanisms in different types of cavitation," Wear **113**, 305 (1986).
[13] R. Young, "Cavitation in pumps, pipes and valves," Process Eng. **71**, 47 (1990).
[14] D. R. Stinebring, "Analysis of cavitation damage on the space shuttle main engine high pressure oxidizer turbopump," ASME Fluids Engineering Division **25**, 71 (1985).
[15] C.-M. Ho and Y.-C. Tai, "Micro-electro-mechanical-systems (MEMS) and fluid flows," Annu. Rev. Fluid Mech. **30**, 579 (1998).
[16] P. Gravesen, J. Branebjerg, and O. S. Jensen, "Microfluidics—a review," J. Micromech. Microeng. **3**, 168 (1993).
[17] H. A. Stone, A. D. Strooch, and A. Ajdari, "Engineering flows in small devices: Microfluidics toward a lab-on-a-chip," Annu. Rev. Fluid Mech. **36**, 381 (2004).
[18] A.-M. Lanzillotto, T.-S. Leu, M. Amabile, R. Wildes, and J. Dunsmuir, "Investigation of microstructure and microdynamics of fluid flow in MEMS," Proceedings ASME Aerospace Division **AD52**, 789 (1996).
[19] M. Madou, *Fundamentals of Microfabrication* (CRC, New York, 1997).
[20] A. P. London, A. A. Ayon, A. H. Epstein, S. M. Spearing, T. Harrison, Y. Peles, and J. L. Kerrebrock, "Microfabrication of a high pressure bipropellant rocket engine," Sens. Actuators, A **A92**, 351 (2001).
[21] A. A. Alexeenko, S. F. Gimelshein, D. A. Levin, A. D. Ketsdever, and M. S. Ivanov, "Measurements and simulation of orifice flow for micropropulsion testing," J. Propul. Power **19**, 588 (2003).
[22] J. Mueller, I. Chakraborty, S. Vargo, C. Marrese, V. White, D. Bame, R. Reinicke, and J. Holzinger, "Towards micropropulsion systems on-a-chip: initial results of component feasibility studies," IEEE Aero. Conference Proceedings, Piscataway, NJ, 2000.
[23] J. Mueller, E.-H. Yang, A. A. Green, V. White, I. Chakraborty, and R. Reinicke, "Design and fabrication of MEMS-based micropropulsion devices at JPL," Proc. SPIE **4558**, 57 (2001).
[24] E. E. Noonan, C. S. Protz, Y. P. Peles, and S. M. Spearing, "Strength analysis of a micro-rocket combustion chamber," Proceedings of Materials Science of MEMS Devices IV Symposium, Boston, MA, 2001.
[25] A. H. Epstein, S. D. Senturia, G. Anathasuresh, A. Ayon, K. Breuer, K.-S. Chen, F. E. Ehrich, G. Gauba, R. Ghodssi, C. Groshenry, S. Jacobson, J. H. Lang, C.-C. Lin, A. Mehra, and J. M. Miranda, "Power MEMS and microengines," Proceedings of Transducers 97 International Conference on Solid-State Sensors and Actuators, Chicago, IL, 1997.
[26] K. Isomura, M. Murayama, and T. Kawakubo, "Feasibility study of gas turbine at microscale," Proceedings of ASME Turbo Exposition, New Orleans, LA, 2001.
[27] L. G. Frechette, "Development of a microfabricated silicon motor-driven compression system," Ph.D. thesis, Massachusetts Institute of Technology, 2000.

[28]J. Burger, H. Holland, E. Berenschot, J.-H. Seppenwodde, M. TerBrake, H. Gardeniers, and M. Elwenspoek, "169 kelvin cryogenic microcooler employing a condenser, evaporator, flow restriction and counterflow heat exchanger," 14th IEEE Conference on MEMS, Piscataway, NJ, 2001.
[29]M. V. Zagarola, J. J. Breedlove, J. A. McCormick, and W. L. Swift, "Turbo-Brayton cryocooler technology for low-temperature space applications," Proc. SPIE **4850**, 1029 (2003).
[30]D.-J. Yao, C.-J. Kim, G. Chen, J. L. Liu, K. L. Wang, J. Snyder, and J.-P. Fleurial, "MEMS thermoelectric microcooler," Proceedings of 20th International Conference on Thermoelectrics, Beijing, China, 2001.
[31]R. Leoni, "On-chip micro-refrigerators for sub-Kelvin cooling," New Astron. Rev. **43**, 317 (1999).
[32]H. Helvajian, P. D. Fuqua, W. W. Hansen, and S. Janson, "Laser microprocessing for nanosatellite microthruster applications," RIKEN Rev. **32**, 57 (2001).
[33]A. A. Ayon, R. L. Bayt, and K. S. Breuer, "Deep reactive ion etching: a promising technology for micro and nanosatellites," Smart Mater. Struct. **10**, 1135 (2001).
[34]S. W. Janson, "Micro/nanotechnology for the satellite world," Proc. SPIE **4981**, 95 (2003).
[35]M. Richter, P. Woias, and D. Weiss, "Microchannels for applications in liquid dosing and flow-rate measurement," Sens. Actuators, A **A62**, 480 (1997).
[36]L. R. Arana, S. B. Schaevitz, A. J. Franz, K. F. Jensen, and M. A. Schmidt, "A microfabricated suspended-tube chemical reactor for thermally efficient fuel processing," J. Microelectromech. Syst. **12**, 600 (2003).
[37]M. W. Losey, R. J. Jackman, S. L. Firebaugh, M. A. Schmidt, and K. F. Jensen, "Design and fabrication of microfluidic devices for multiphase mixing and reaction," J. Microelectromech. Syst. **11**, 709 (2002).
[38]J. P. Blanchard, D. L. Henderson, A. Lal, H. Li, and S. Santanam, "Radioisotope power for MEMS devices," Trans. Am. Nucl. Soc. **86**, 186 (2002).
[39]D. Huh, H. H. Wei, J. B. Grotberg, S. J. Skerlos, K. Kurabayashi, and S. Takayama, "Use of air-liquid two-phase flow in hydrophobic microfluidic channels for disposable flow cytometers," Biomed. Microdevices **4**, 141 (2002).
[40]A. Marshall and J. Hodgson, "DNA chips: An array of possibilities," Nat. Biotechnol. **16**, 27 (1998).
[41]R. C. Anderson, G. J. Bogdan, Z. Bamiv, T. D. Dawes, J. Winkler, and K. Roy, "Microfluidic biochemical analysis system," Proceedings of International Conference on Solid-State Sensors and Actuators, Chicago, IL, 1997.
[42]J. W. Holl, "Nuclei and cavitation," J. Basic Eng. **92**, 681 (1970).
[43]S. Pennathur, "Micro-scale turbopump blade cavitation," M.S. thesis, Massachusetts Institute of Technology, Cambridge, MA, 2001.
[44]S. Pennathur, Y. Peles, and A. H. Epstein, "Cavitation at micro-scale in MEMS fluid machinery," Proceedings of ASME International Mech. Engg. Congress and Exposition, New Orleans, LA, 2002.
[45]R. W. Kermeen, J. T. McGraw, and B. R. Parkin, "Mechanism of cavitation inception and related scale-effects problem," Proceedings of ASME Meeting MEX-1, New York, NY, 1954.
[46]J. W. Holl and G. F. Wislicenus, "Scale effects on cavitation," J. Basic Eng. **83**, 385 (1961).
[47]C.-T. Hsiao, G. L. Chahine, and H.-L. Liu, "Scaling effect on prediction of cavitation inception in a line vortex flow," J. Fluids Eng. **125**, 53 (2003).
[48]A. P. Keller, "Scale effects at beginning cavitation applied to submerged bodies," ASME Fluids Engineering Division **16**, 43 (1984).
[49]G. L. Chahine, "Cavitation dynamics at microscale level," J. Heart Valve Dis. **3**, 102 (1993).
[50]D. R. Stinebring, R. E. A. Arndt, and J. W. Holl, "Scaling of cavitation damage," J. Hydronautics **11**, 67 (1977).
[51]M. L. Billet and J. W. Holl, "Scale effects on various types of limited cavitation," J. Fluids Eng. **103**, 405 (1981).
[52]Y. Kuhn de Chizelle, S. L. Ceccio, and C. E. Brennen, "Observations and scaling of traveling bubble cavitation," J. Fluid Mech. **293**, 99 (1995).
[53]T. Hasegawa, M. Suganuma, and H. Watanabe, "Anomaly of excess pressure drops of the flow through very small orifices," Phys. Fluids **9**, 1 (1997).
[54]J. Pfahler, J. Harley, H. Bau, and J. Zemel, "Liquid transport in micron and submicron channels," Sens. Actuators, A **A22**, 431 (1990).
[55]P. Woias, "Micropumps-summarizing the first two decades," Proc. SPIE **4560**, 39 (2001).
[56]L. Saggere, N. W. Hagwood, D. C. Roberts, H.-Q. Li, J. L. Steyn, K. Turner, J. A. Carretero, O. Yaglioglu, Y.-H. Su, R. Mlcak, S. M. Spearing, K. S. Breuer, and M. A. Schmidt, "Design, fabrication, and testing of a piezoelectrically driven high flow rate micro-pump," Proceedings of 12th IEEE International Symposium on Applications of Ferroelectrics, Honolulu, HA, 2001.
[57]H. Q. Li, D. C. Roberts, J. L. Steyn, K. T. Turner, O. Yaglioglu, N. W. Hagood, S. M. Spearing, and M. A. Schmidt, "Fabrication of a high frequency piezoelectric microvalve," Sens. Actuators, A **A111**, 51 (2004).
[58]D. C. Roberts, H. Q. Li, J. L. Steyn, K. T. Turner, R. Mlcak, L. Saggere, S. M. Spearing, M. A. Schmidt, and N. W. Hagood, "A high-frequency, high-stiffness piezoelectric actuator for microhydraulic applications," Sens. Actuators, A **A97–A98**, 620 (2002).
[59]D. J. Laser and J. G. Santiago, "A review of micropumps," J. Micromech. Microeng. **14**, R35 (2004).
[60]A. K. Henning, J. Fitch, D. Hopkins, L. Lilly, R. Faeth, E. Falsken, and M. Zdeblick, "A thermopneumatically actuated microvalve for liquid expansion and proportional control," Tranducers 97 International Conference on Solid-State Sensors and Actuators, Chicago, IL, 1997.
[61]X. N. Jiang, Z. Y. Zhou, X. Y. Huang, Y. Li, Y. Yang, and C. Y. Liu, "Micronozzle/diffuser flow and its application in micro valveless pumps," Sens. Actuators, A **A70**, 81 (1998).
[62]X. Y. Ye, F. Tang, H. Q. Ding, and Z. Y. Zhou, "Study of a vaporizing water micro-thruster," Sens. Actuators, A **A89**, 159 (2001).
[63]J. A. Carretero and K. S. Breuer, "Measurement and modeling of the flow characteristics of micro disc valves," Proceedings of MEMS 2000 ASME International Mech. Engg. Congress and Exposition, Orlando, FL, 2000.
[64]S. L. Anna, N. Bontoux, and H. A. Stone, "Formation of dispersions using flow focusing in microchannels," Appl. Phys. Lett. **82**, 364 (2003).
[65]S. Baik, J. P. Blanchard, and M. L. Corradini, "Development of microdiesel injector nozzles via microelectromechanical systems technology and effects on spray characteristics," J. Eng. Gas Turbines Power **125**, 427 (2003).
[66]W. Y. Lee, M. Wong, and Y. Zohar, "Pressure loss in constriction microchannels," J. Microelectromech. Syst. **11**, 236 (2002).
[67]Y. Yan and R. B. Thorpe, "Flow regime transitions due to cavitation in the flow through an orifice," Int. J. Multiphase Flow **16**, 1023 (1990).
[68]J. W. Ball, J. P. Tullis, and T. Stripling, "Predicting cavitation in sudden enlargements," ASCE J. Hydraul. Div. **101**, 857 (1975).
[69]J. P. Tullis, "Choking and supercavitating valves," ASCE J. Hydraul. Div. **97**, 1931 (1971).
[70]J. P. Tullis and R. Govindarajan, "Cavitation and size scale effect for orifices," ASCE J. Hydraul. Div. **99**, 417 (1973).
[71]F. Numachi, M. Yamabe, and R. Oba, "Cavitation effect on the discharge coefficient of the sharp-edge orifice plate," J. Basic Eng. **82**, 1 (1960).
[72]J. W. Daily and D. R. F. Harleman, *Fluid Dynamics* (Addison-Wesley, Reading, MA, 1966).
[73]K. Ramamurthi and K. Nandakumar, "Characteristics of flow through small sharp-edged cylindrical orifices," Flow Meas. Instrum. **10**, 133 (1999).
[74]T. S. Koivula and A. U. Ellman, "Cavitation behavior of hydraulic orifices and valves," SAE Trans. **107**, 387 (1998).
[75]Z. Bikai, H. Yan, T. Zhang, and L. Zhuangyun, "Experimental investigation of the flow characteristics of small orifices and valves in water hydraulics," J. Process Mech. Engg. **216**, 235 (2002).
[76]K. Ramamurthi and S. R. Patnaik, "Influence of periodic disturbances on inception of cavitation in sharp-edged orifices," Exp. Fluids **33**, 720 (2002).
[77]N. H. Nurick, "Orifice cavitation and its effect on spray mixing," J. Fluids Eng. **98**, 681 (1976).
[78]A. Yamaguchi and T. Suzuki, "Cavitation in hydraulic fluids. Part 3: On cavitation in long orifices," J. Fluid Control **12**, 21 (1980).
[79]I. D. Pearce and A. Lichtarowicz, "Discharge performance of long orifices with cavitating flow," Proceedings of Second Fluid Power Symposium, Guildford, UK, 1971.
[80]J. P. Tullis, *Hydraulics of Pipelines* (Wiley, New York, 1989).
[81]S. J. Kline and F. A. McClintock, "Describing uncertainties in single-sample experiments," Mech. Eng. (Am. Soc. Mech. Eng.) **75**, 38 (1953).
[82]J. G. Santiago, S. T. Wereley, C. D. Meinhart, D. J. Beebe, and R. J. Adrian, "Particle image velocimetry system for microfluidics," Exp. Fluids **25**, 316 (1998).
[83]S. Devasenathipathy, J. G. Santiago, S. T. Wereley, C. D. Meinhart, and K. Takehara, "Particle imaging techniques for microfabricated fluidic systems," Exp. Fluids **34**, 504 (2003).

[84]G. L. Chahine and Y. T. Shen, "Cavitation bubbles near boundaries." J. Fluids Eng. **108**, 99 (1986).
[85]H. B. Marschall, K. A. Mørch, A. P. Kellar, and M. Kjeldsen, "Cavitation inception by almost spherical solid particles in water," Phys. Fluids **15**, 545 (2003).
[86]S. Gopalan, J. Katz and O. Knio, "The flow structure in the near field of jets and its effect on cavitation inception," J. Fluid Mech. **398**, 1 (1999).
[87]D. P. Schmidt and M. L. Corradini, "Analytical prediction of the exit flow of cavitating orifices," Atomization Sprays **7**, 603 (1997).
[88]J. W. Holl and A. L. Treaster, "Cavitation hysteresis," Proceedings ASME Meeting FE-9, New York, NY, 1965.
[89]V. H. Arakeri, J. A. Carroll, and J. W. Holl, "A note on the effect of short and long laminar separation bubbles on desinent cavitation," J. Fluids Eng. **103**, 28 (1981).
[90]J. W. Holl, "Effect of air content on occurrence of cavitation," J. Basic Eng. **82**, 941 (1960).
[91]R. E. A. Arndt and A. P. Keller, "Water quality effects on cavitation inception in a trailing vortex," J. Fluids Eng. **114**, 430 (1992).